Comparing Quantitative and Psychophysical Methods of Resolution Assessment in Digital Radiology

MSc Project Report

Department of Medical Physics & Bioengineering
University College London

Michael Hughes

August 2011

Word Count: 9600

Abstract

Routine quality assurance checks on medical x-ray detectors in UK hospitals typically involve psychophysical measurement of spatial resolution using the Huttner line pair phantom. There has recently been increased interest in adopting more quantitative measures, such as the modulation transfer function (MTF), for this purpose. In this study the results of Huttner measurements of limiting spatial resolution are compared to direct measurements of the MTF using a tungsten edge. A relationship is derived to convert tolerances applied to Huttner measurements to tolerances on measurements of MTF50 and MTF10. This allows the relative repeatability and reproducibility of the two methods to be directly compared. The current IPEM recommended tolerance of two Huttner line pair groups is shown to be equivalent to a 20% change in MTF50 or MTF10 for a Gaussian MTF. An analysis of uncertainties in the measured MTF shows them to be less than 5%, demonstrating that this approach is several times more sensitive to changes in spatial resolution than psychophysical methods.

Author's Contact Details:

michael.robert.hughes@gmail.com

Acknowledgements

I would like to thank all those who provided help, support and advice to me whilst I was working on this project. In particular thanks must go to my supervisor, Mary Cocker, who was highly supportive of what I was doing, but who allowed me free reign to explore the avenues I was most interested in. Thanks also to Andrew Reilly, who loaned me the tungsten square used for the MTF measurements, and whose PhD thesis and IQWorks software proved invaluable.

This work relied on a number of people, both at the Churchill Hospital and elsewhere, taking the time to score a set of phantom images, and I am grateful for their contribution. Elements of this work were presented at the IPEM Quantitative Image Analysis workshop in October 2010 and I received a great deal of useful feedback which helped to guide the direction the project was taking. I hope that the results of this work will contribute something of value to the medical physics community.

Note

Corrections have been made to this manuscript following comments at the viva voce examination, particularly to correct errors in the mathematics in Section 5.

Contents

1 Introduction

The *Ionising Radiation Regulations* (1999) require that regular quality assurance tests are performed on diagnostic x-ray devices. The purpose of these tests is to ensure that radiation doses received by patients during exposures are 'as low as reasonably practicable'. Checks are performed on the x-ray tube, radiation shielding and automatic exposure controls as well as on the detector or film-screen system (IPEM 2005). The detector tests satisfy legislation by ensuring that exposures are optimised with respect to radiation dose, and confirm that consistently high quality radiographs are being produced.

Report 91 from the Institute of Physics and Engineering in Medicine, "*Recommended Standards for the Routine Performance Testing of Diagnostic X-Ray Imaging Systems*," (IPEM 2005) identifies a number of metrics which can be used to quantify the performance of detectors. These include 'threshold contrast detail detectability' (TCDD), a measure of how well faint objects of various sizes can be observed, and limiting spatial resolution (LSR), a measure of how well closely spaced objects can be resolved. These metrics have found applications in the characterisation and comparison of different detectors (see for example Rong *et al*. 2011), and are commonly used in UK hospitals for monitoring the long term performance of a single detector (IPEM 2005, IPEM 2010). They also contribute to the decision over whether a new installation meets the manufacturer's specifications and whether it is fit for clinical use, and so play an important role in patient protection.

A key feature of these traditional metrics is that they rely on an observer scoring images of test phantoms. The tests are described as psychophysical (Beutal 2000), in the sense that they measure the performance of the observer as well as of the detector. In some respects this can be considered an advantage, as it means that changes in physical performance are measured in terms of observable changes in the image. However, a high level of consistency of scoring between different observers, and even between the same observer at different times, can be hard to achieve, making it difficult to reliably detect small changes in performance. For example, a study by Cohen *et al.* (1984) suggested that the likely error when scoring TCDD phantoms is of the order of 22% for a single observer, and remains as high as 12% even if an average is taken of results from four different observers.

In the last few years film-screen systems have become largely obsolete, being replaced firstly by computed radiography (Rowlands 2002) and more recently by direct digital detectors (NHS 2007). These developments have made computerised analysis of image quality more practical, and there has been interest in establishing quality assurance protocols using quantitative metrics (Metz *et al*. 1994, Marshall 2007, Cunningham 2008, Marshall 2009, IPEM 2010, Marshal *et al.* 2011). Examples of such metrics include the modulation transfer function (MTF), the noise power spectrum (NPS) and a combination of the two: the detective quantum efficiency (see Dobbins 2006 for a review). While these methods have been used for the characterisation of systems for many years (see for example Launders *et al.* 1998, Samei and Flynn 2003), their use in regular QA has not yet been fully established (IPEM 2010).

Whilst work on this project was underway, IPEM published an updated volume of its Report 32, entitled "*Measurement of the performance characteristics of diagnostic x-ray systems: digital imaging systems*" (IPEM 2010). This document suggests using the MTF and NPS metrics in routine quality assurance of digital x-ray detectors, but falls short of recommending that they should entirely replace psychophysical methods. It does however, provide standardised methods for measuring these two quantities.

One key question which was not fully addressed by the report is how best to use quantitative metrics in such a way as to ensure consistency of standards with existing methods. If quantitative analysis is to have a meaningful role in quality assurance then tolerances for these metrics must be established. This allows the significance of a given change in performance to be understood, and aids decisions on whether or not corrective action should be taken. IPEM Report 91 (IPEM 2005) defines two types of tolerance: remedial, which indicates that some attention is necessary in the near future, and suspension, which requires that the unit is immediately removed from clinical use. The tolerances are usually expressed as a change in performance relative to 'baseline' values which are acquired during equipment installation and commissioning.

The process of setting tolerances for psychophysical methods is simplified by the element of human involvement in the measurement. If the observer is able to reliably detect a change in a phantom image then that change can be considered significant in the sense that it corresponds to an observable change in image quality. This approach is less practical for determining tolerances for quantitative metrics. There may not be a simple relationship between a given change and its effect on human perception of the image (Loo *et al.* 1984, Myers *et al.* 1985, Cunningham and Shaw 1999), although several studies have

suggested that such relationships exist in principle (Chesters and Hay 1983, Good *et al.* 1994, Marshall 2006).

One approach to setting tolerances for quantitative metrics is to collect data over a period of time and then select a tolerance sufficiently relaxed so that random variations (for example due to differences in set-up) will not cause it to be breached. If sufficient care is taken with measurements then this may lead to tolerances which are significantly tighter than those for psychophysical scoring, and which correspond to changes sufficiently small that they cannot be detected visually. It may then be difficult to justify taking expensive or disruptive action in response to a breach of these tolerances when there is no obvious observable change in image quality.

In this report the relationship between commonly used quantitative and psychophysical spatial resolution metrics is investigated. In particular, the tilted edge method of measuring MTF is compared to manual scoring of the Huttner LSR test object. An expression is derived which relates tolerances for these two metrics and, although the relationship is mathematically valid only for particular limited cases, it is shown that it has practical application across a wide range of situations. This allows the relative reproducibility of the two methods to be compared, and it is shown that measurements of the MTF are generally much more sensitive to changes in detector resolution. These results may be of use in assisting hospitals in setting local tolerances for quantitative quality assurance programmes.

2 Background

The performance of digital imaging systems can be described in terms of two physical properties: spatial resolution and noise (Metz *et al*. 1994, IPEM 2010). Both quantitative and psychophysical approaches to image quality assessment seek to measure these properties in some way. As will be described below, the modulation transfer function (MTF) is dependent only on the spatial resolution, whereas the limiting spatial resolution (LSR) may also depend on the level of noise present, and must be measured under strictly reproducible conditions.

2.1 Resolution in Linear Imaging Systems

A convenient way to characterise the resolution of an imaging system is to formulate a description of how it transmits an infinitesimally small point (or 'impulse') object. A perfect imaging system would produce an image which is an exact replica of the point object, whereas any real imaging system will produce what we might describe as a 'blurred' representation (Suetens 2002). This blurred image of a point object is known as the point spread function, or PSF, and in many cases is sufficient to provide a complete description of the imaging system's resolution (Beutel 2000).

For a two dimensional detector one could (in principle) define a PSF for each point. An arbitrary 2D input, which we will label the object, can be represented as a weighted sum of a number of these point sources. If the imaging system is linear (i.e. if the image intensity is proportional to the object intensity), and a gain of unity is assumed for simplicity, then the intensity of each point on the image, $I_{x,y}$, can be computed from the sum (Metz and Doi 1979):

$$I_{x,y} = \sum_{x',y'} O_{x,y} \cdot PSF_{x,y}(x', y'), \qquad 2\text{-}1$$

where, $O_{x,y}$ is the object intensity at point (x, y) and $PSF_{x,y}(x', y')$ is the 2D point spread function centred on the point (x, y) and defined over the full range of (x', y') The resulting image is therefore a weighted sum of the PSFs for all points which make up the image.

For practical purposes it is often convenient to assume that the PSF is identical for all points on the detector, a property known as shift invariance. In this case, the summation of Equation 2-1 can be replaced with a convolution:

$$I = O \otimes PSF \,. \qquad 2\text{-}2$$

Combined with an assumption that there is no change in resolution with time, this relation defines what is known as a linear, time-independent (LTI) system (Metz and Koi 1979).

We can consider the convolution with the PSF to be an operator (which we shall label A) acting on the object. For simplicity we shall work in one dimension only, but the results are easily generalised to higher dimensions. We can then search for a set of eigenfunctions, f, of this operator, such that:

$$Af = \lambda f \,, \qquad 2\text{-}3$$

where λ is a constant. If A is an LTI operator then it is trivial to show that $f(x) = \exp(iax)$ is an eigenfunction for all a. Sinusoidal functions, which can be expressed as sums of complex exponentials, are therefore eignenfunctions of the LTI convolution operator. This means that, for an object represented as a sinusoid of spatial frequency υ, the image is a sinusoid with the same frequency but a (possibly) different amplitude.

It is computationally efficient to compute convolutions in the Fourier domain by making use of the convolution property of the Fourier transform (Reilly 2010). For a 2D system we have:

$$\Im(I) = \Im(O) \times \Im(PSF) \,, \qquad 2\text{-}4$$

where $\Im$ denotes the Fourier transform. It is now clear that the relative change in amplitude for a sinusoid of spatial frequency υ is given by the magnitude of $\Im(PSF)$ at the particular values of υ. Since, from Fourier theory, any function can be represented as a summation of sinusoids of different spatial frequencies, knowing $\Im(PSF)$ for all υ allows us to compute how any function is transferred from the object to the image.

This useful property means that the magnitude of Fourier transform of the point spread function, $|\Im(PSF)|$, is a convenient way to describe the resolution of an imaging

system. The 2D Fourier transform of the 2D PSF is known as the modulation transfer function, or MTF (see for example Samei *et al*., 2006). The MTF describes the attenuation in amplitude of sinusoidal objects of different spatial frequencies by the imaging system. It is normalised so that its value at zero spatial frequency is 1:

$$MTF(u,v) = \frac{\Im\{PSF(x,y)\}}{\Im\{PSF(x,y)\}\big|_{u=v=0}}. \qquad 2\text{-}5$$

As with the PSF, it is often practical to assume the MTF is isotropic. In this case, the PSF can be integrated along one spatial dimension to yield the line spread function, LSF, and the Fourier transform of the LSF is the one dimensional (1D) MTF. It is important to note that the Fourier transform of a profile taken through the 2D PSF is not equivalent to the 1D MTF. For isotropic MTFs, the two are, however, related by the Hankel and Abel transforms (Metz and Koi 1979).

2.1.1 Limiting Spatial Resolution

The limiting spatial resolution (LSR) of an imaging system is a measurement of the highest frequency modulation which is discernable in the image. Although widely used for hospital quality assurance purposes (IPEM 2005), it is in some respects a poorly defined concept which may be dependent on system properties other than the MTF (Marshall *et al*. 2011).

This can be illustrated by considering a hypothetical classical imaging system (which in this context will be taken to mean that there is no quantisation) with zero noise. We shall assume that the lack of quantisation extends to the spatial dimensions, so that there are no pixels or other forms of granularity. Note that this does not necessarily imply infinite resolution, but merely infinitely fine sampling. The transfer of a sinusoidal pattern of a given spatial frequency through such an imaging system is simple to compute – the amplitude of the modulation is simply scaled by the value of the MTF at that frequency. For an MTF which is greater than zero for all spatial frequencies (for example a Gaussian) there is no spatial frequency for which the modulation is reduced to zero. Providing that there are no limitations on the ability of the observer to window the image (i.e. to scale the gray values on his monitor), line pairs of arbitrarily small separation can be distinguished. The observer would therefore conclude that the limiting resolution of the system is infinite.

In practice, all imaging system will contain noise. Even if a perfect photon counting detector was available, the resulting image would still be subject to quantum mechanical noise arising from an inherent randomness in the emission of radiation. This magnitude of this 'quantum mottle' relative to the signal can be reduced by increasing the number of photons striking the detector, but it can never be removed entirely. The effect is to limit the ability of the observer to distinguish small modulations from the background of the random variations. It is reasonable to assume that, under fixed observing conditions, there will be a limiting modulation contrast-to-noise ratio (CNR), beyond which the observer can no longer reliably detect the presence of a modulation (Schober and Hilz 1965). This critical ratio is not a fundamental physical quantity, but is dependent on the ability of the observer to distinguish signal from noise.

2.1.2 Psychophysical Determination of Limiting Spatial Resolution

Limiting spatial resolution can be determined experimentally by imaging a test object consisting of groups of line pairs of varying pitch (i.e. a varying number of line pairs per mm). The observer assesses the highest spatial frequency line pair group for which they can resolve the individual lines with out aliasing. A commonly used object is the Huttner test object (IPEM 2005, IPEM 2010), which is shown in Figure 3-2. For the purposes of the present work, a specific version of this test object will be considered. The Huttner-21 consists of 21 line pair groups, with pitches as listed in Table 2-1. However, all results can easily be generalised to other, similar test patterns.

Group	Line pairs/mm	Pitch (mm)
1	0.50	2.00
2	0.56	1.79
3	0.68	1.47
4	0.71	1.41
5	0.80	1.25
6	0.90	1.11
7	1.00	1.00
8	1.12	0.89
9	1.25	0.80
10	1.40	0.71
11	1.60	0.63
12	1.80	0.56
13	2.00	0.50
14	2.24	0.45
15	2.50	0.40
16	2.80	0.36
17	3.15	0.32
18	3.55	0.28
19	4.00	0.25
20	4.50	0.22
21	5.00	0.20

Table 2-1: Data for Huttner-21 LSR test object. There are a total of 21 line pair groups, with a broadly consistent change in line pair spacing between each group.

Instructions for reading such test objects in the UK are provided by IPEM (IPEM 2010). It suggests tilting the object to 45 degrees with respect to the pixel matrix to reduce the effects of aliasing, and states the limiting spatial resolution should approach the Nyquist frequency for most detectors (see Section 2.1.4).

2.1.3 Square Wave Contrast Function

Sinusoids are the eigenfunctions of the resolution transfer function, and so a natural function with which to measure resolution. However, for engineering reasons it is rare for sinusoidal test patterns to be produced (Nill 2001). Commonly used test patterns, such as the Huttner, use square waves, as shown in profile in Figure 2-1(a). Square waves are not, in general, eigenfunctions of the PSF convolution function. The shape of the modulation is therefore changed by the imaging system, and the amplitude of modulation of a given square wave frequency in the image is not equal to the MTF for that spatial frequency.

The Fourier transform of a square wave function is shown in Figure 2-1. It can be seen that the Fourier components consist of a primary harmonic plus higher order harmonics at regular intervals. For a square wave test pattern that has a spatial frequency close to the limiting spatial resolution, a significant simplification can be made. Providing that the imaging system is not over-sampled, all harmonics other than the principle are likely to lie beyond the Nyquist frequency and will not be sampled. The Fourier domain representation of the test pattern is therefore identical in shape (although not in amplitude) to that for a sign wave with the same spatial frequency. A square-wave test pattern at the limiting spatial frequency will be transformed into a sine wave in the image.

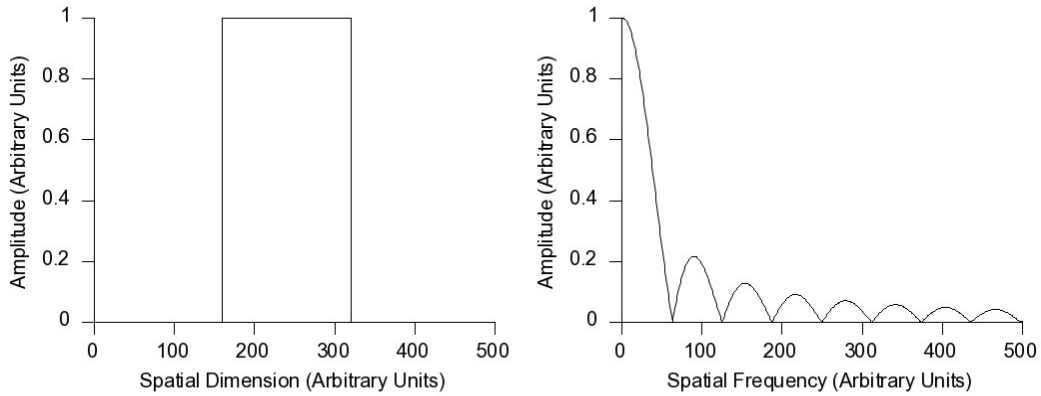

Figure 2-1: (a) Single square wave, (b) Fourier transform of the square wave.

If we measure the amplitude of the sinusoid in the image and compare it with the amplitude of the object square wave we can compute, by analogy to the MTF, the square wave contrast function (SWCF) (Coltmann 1954). Like the MTF, the SWCF will generally decrease with spatial frequency, υ (although for an arbitrary PSF the decrease may not be

monotonic). When limiting spatial resolution, $\upsilon_{\lim}$, is measured by the Huttner Object, the observer is therefore judging the value of υ for which $SWCF(\upsilon)$ falls below some threshold, T.

It must be stressed that the SWCF is not identical to the MTF, even in the region of $\upsilon_{\lim}$. However, Coltman (1954) has demonstrated that the two are related by an infinite series. In the region near the limiting spatial resolution, it has been shown (Campbell and Robson 1968, Nill 2001) that this can be simplified to:

$$MTF(\upsilon) = \frac{\pi}{4} SWCF(\upsilon) \quad \text{for } \upsilon \sim \upsilon_{\lim}. \qquad 2\text{-}6$$

This theory suggests that, for or a given set of observing conditions, $\upsilon_{\lim}$ can be determined from $T = SWCF(\upsilon_{\lim})$, where T is some threshold. Using Equation 2-6, and providing T is known, it should therefore be possible to determine at least one point on the MTF curve from a psychophysical measurement of $\upsilon_{\lim}$. Experimental measurements of T are reported in Section 6.3, but, more importantly it will be shown in Section 5 that uncertainty on the psychophysical determination of $\upsilon_{\lim}$ can be converted to uncertainty on the predicted $MTF(\upsilon_{\lim})$ without knowing T.

2.1.4 Effects of Pixel Size

In discussions so far it has been assumed that the pixel sampling is infinitely fine. In practice the pixel size may be sufficiently large so that is comparable to the width of the PSF, and hence has a significant effect on the apparent resolution (Dobbins 1995).

The Nyquist-Shannon sampling theorem (Shannon 1949) states that a signal must be sampled at a rate equal to at least twice the highest frequency present in the signal in order for it to be reproduced faithfully. This frequency is known as the Nyquist frequency. In the case of an x-ray detector, modulations in the object with a pitch less than twice the pixel pitch will therefore not be faithfully reproduced in the image, but, as described below, may be aliased to appear as lower frequencies.

The effects of pixel sampling may be represented as a two-step process (Goodman 2005). The first is a convolution with a function describing the sensitivity profile of each pixel. For the purposes of this discussion, this profile will be assumed to be rectangular

(rect) function with a width equal to the pixel pitch – this is equivalent to a 100% fill factor. The second step is a sampling using a Dirac delta comb. In 1D, we have:

$$\mathrm{PSF}_{\text{sampled}}(x) = \left[\mathrm{PSF}_{\text{pre-sampling}}(x) \otimes \mathrm{rect}\left(\frac{x}{s}\right) \right] \times \mathrm{III}\left(\frac{x}{d}\right), \qquad 2\text{-}7$$

where rect is the rectangular function:

$$\mathrm{rect}\left(\frac{x}{d}\right) = \begin{cases} 0 & \text{for } |x/d| > 1/2 \\ 1/2 & \text{for } |x/d| = \pm 1/2 \\ 1 & \text{for } |x/d| < 1/2 \end{cases}, \qquad 2\text{-}8$$

III is the dirac comb:

$$\mathrm{III}\left(\frac{x}{d}\right) = \sum_{k=0}^{\infty} \delta(x - kd), \qquad 2\text{-}9$$

d is the pixel pitch, s is the pixel size ($s = w$ for 100% fill factor), and x is the spatial co-ordinate. The Fourier transform of the sinc function is a sinc, and the Fourier transform of the Dirac comb is another comb:

$$\Im\left\{\mathrm{III}\left(\frac{x}{d}\right)\right\} = III(d\varpi), \qquad 2\text{-}10$$

where ω is spatial frequency. The MTF will therefore be given by (Dobbins 1995):

$$\mathrm{MTF}_{\text{sampled}} = \left| \Im\left\{\mathrm{PSF}_{\text{pre-sampling}}\right\} \times \mathrm{sinc}(\mathrm{d}\varpi) \right| \otimes \mathrm{III}(\mathrm{d}\omega). \qquad 2\text{-}11$$

We have introduced two additional terms to the expression for MTF. The sinc term results in an additional attenuation factor at higher frequencies. Since the Nyquist frequency is given by $\omega = 1/(2d)$, the fall-off in MTF from the sinc term at this point is $\sin(\pi/2)/(\pi/2) \approx 0.64$. Any attempt to estimate the pre-sampling MTF from an MTF calculated from a sampled system must therefore take account of this effect.

The comb function in Equation 2-11 causes an additional complication known as aliasing. The effect of a convolution of a function with a comb is to introduce replicas of the function at intervals equal to the pitch of the comb (Dobbins 1995). When these

replicas overlap there is no simple method to recover the original, separate signals. The effect in the spatial domain is that modulations in the object with frequencies higher than the Nyquist frequency appear as lower frequency modulations in the image.

Since the pitch of the comb in the Fourier domain is inversely proportional to the pitch of the sampling comb in the spatial domain, coarser sampling will lead to a worsening of this effect. Some aliasing will occur whenever the pre-sampling MTF has non-zero amplitude for frequencies above the Nyquist frequency. The effect is particularly noticeable with regular modulations with such as the Huttner test patterns.

A further effect of the comb function is a loss of shift invariance (Dobbins 1995). From Equation 2-11 it is clear that adjusting the phase of the sampling array relative to the object (i.e. changing the value of x in Equation 2-9) will alter the resulting measured MTF. If the MTFs from all possible phase shifts are averaged, the 'expectation MTF' is obtained (Dobbins 1995). However, the expectation MTF is dependent on the input (object) signal and will certainly not correctly describe the response to a single sinusoid of a given frequency (Beutal 2000). Instead, it is more practical to measure the pre-sampling MTF – the MTF that would occur if there was no pixel sampling. For psychophysical measurements, the effects of aliasing and shift-dependence are mitigated somewhat by imaging the test object at an angle, typically at 45 degrees (IPEM 2010).

2.1.5 Direct Measurement of the MTF

In general, one wishes to measure the pre-sampling MTF - the MTF before pixel sampling occurs (IPEM 2010). The sampled MTF can then easily be determined by multiplication by the sinc function corresponding to the pixel size. In contrast, it is more difficult to calculate the pre-sampling MTF from the sampled MTF since the required deconvolution would tend to amplify noise, and because of the shift invariance problems discussed above.

The sampled MTF is given by the Fourier transform of a profile taken across an image of a line object of infinitesimal thickness (known as the line spread function, LSF). The pre-sampling, shift invariant, MTF can be approximated by angling the line a small amount (typically 10 degrees) with respect to the pixel matrix (Cunningham 1991, Fujita *et al.* 2002). If a profile is now taken along the pixel matrix, the line is effectively sampled at much higher pixel rate. Providing the angle is known, the true distance scale of the profile can easily be calculated from simple trigonometry.

In practice it is difficult to produce a low noise image of anything approximating an infinitesimally thin line (Cunningham 1991). However, if a profile is taken across an edge, then this edge spread function (ESF) can be differentiated to obtain the LSF. As differences are being taken, this process can tend to amplify noise in the ESF, and so some form of smoothing may be applied. A function is also often fitted to the tails of the LSF to ensure that they are brought smoothly to zero (IPEM 2010, Reilly 2010). IPEM has recently published a recommended method for use in the UK for measuring pre-sampling MTF (IPEM 2010).

3 Methods

MTF and limiting spatial resolution were compared using computer simulations and physical measurements. Simulations involved the generation of an artificial Huttner radiograph as described in Section 3.1. Physical measurements of the resolution of a GE Definium 8000 direct digital detector were made using both MTF and Huttner, as described in Sections 3.3 and 3.4. The reproducibility of the MTF was assessed by repeated measurement and by altering measurement conditions, whilst the Huttner reproducibility was assessed by recruiting a number of volunteers to score the same images. Wherever possible, standardised experimental methods and software packages were used to ensure compatibility with current practice in the UK.

3.1 Simulations

Simulations of the Huttner phantom were performed using GNU Octave v3.2.4, an open-source alternative to Matlab (Mathworks). Line pair elements were assumed to have a rectangular profile and a length of 10 mm. For simulations where realistic noise was required, this was added by randomly selecting values from a Poisson distribution. The heel effect and other structural noise sources were not modelled.

Images were generated using a high pixel sampling rate of 30 pixels per mm. The effects of finite PSF were modelled by convolving the Huttner images with a normalised kernel corresponding to the desired PSF, followed by down-sampling to achieve the required pixel size.

3.2 Measurement Conditions

The chest detector of a GE Definium 8000 x-ray unit was used for all physical measurements. This detector consists of an amorphous silicon (a-Si) array covered with a thallium doped sodium iodide scintillator. When x-rays strike the scintillator visible photons are generated, some of which are then detected by the a-Se array. This type of detector is energy integrating, rather than photon counting, which has a small effect on noise statistics but which does not directly affect the resolution.

The detector pixel size was 0.2 mm, with an almost 100% fill factor. The pixel matrix size was 2022 x 2022 pixels, equivalent to an approximately 40 x 40 cm active area. The anti-scatter grid was removed for all exposures, and parameters were set manually rather than using the automatic exposure control. Following acquisitions of radiographs, the raw (unprocessed images) were exported in 14 bit monochrome DICOM format.

For quantitative measurements it is a requirement that the image pixel values scale linearly with dose (IPEM 2010). The relationship between pixel value and dose (known as the signal transfer property, STP) was measured using a Barracuda dosemeter. The dosimeter was placed on the floor with the x-ray field collimated to it in order to reduce the effects of backscatter. Exposures were made at 90 kV for eight different current-time products spread between 0.5 and 32 mAs, and the dose (air kerma) was measured for each. The exposures where then repeated with the x-ray tube pointed at the chest detector, resulting in a set of eight radiographs. The mean pixel value in each image was measured in a 100 x 100 pixel square at the centre of the image.

Figure 3-1 shows the mean pixel value plotted against air kerma (detector dose). This demonstrates that the STP is linear to within the precision of the measurement. Had the STP not been linear then it would have been necessary to linearise the pixel values in each image by applying the inverse of the measured STP (IPEM 2010).

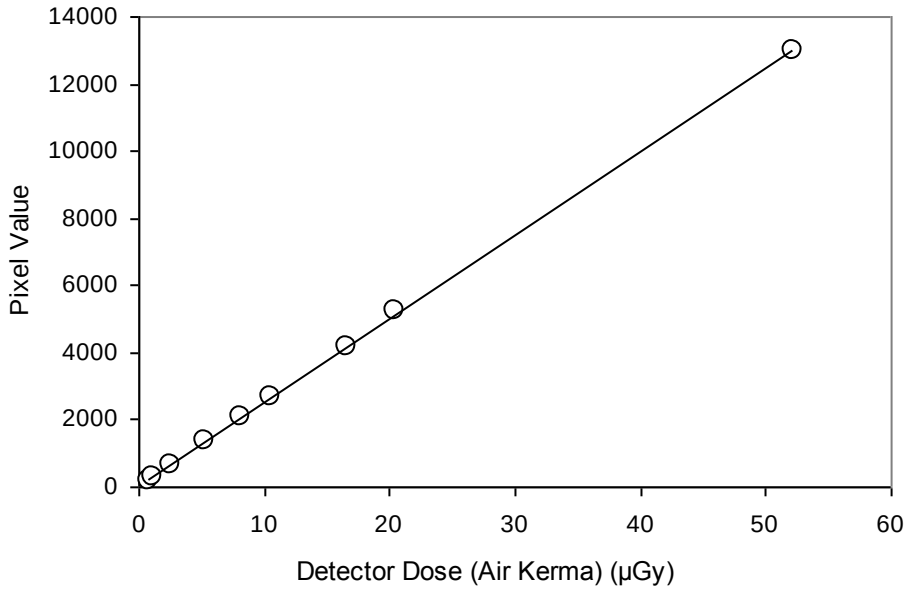

Figure 3-1: Signal transfer property (STP) for Definium 8000 chest detector.

3.3 Psychophysical Measurements

Real and simulated images of the Huttner phantom were scored by volunteers in two separate scoring studies. Where possible, calibrated monochrome monitors were used to view the images, although some scoring was performed on conventional workstations. The observer was free to adjust the level and window of the image and the zoom. The observers were instructed to consider a line pair group irresolvable if obvious aliasing was occurring.

3.3.1 Main Scoring Study

A single radiograph of the Huttner test object was acquired with exposure parameters of 70 kV, 10 mAs, 1 mm added copper filtration and a 150 cm source to detector distance. Two additional Huttner images were then created by applying Gaussian smoothing filters of radius (Gaussian standard deviation) 0.1 and 0.2 mm. The properties of these three images are summarised in Table 3-1 and an example image is shown in Figure 3-2(a).

Image Number	Test Object	Details
1	Huttner-21	70 kV, 10 mAs, 1 mm added Cu filtration.
2	Huttner-21	As Image 1 with Gaussian filter (σ = 0.1 mm) applied.
3	Huttner-21	As Image 1 with Gaussian filter (σ = 0.2 mm) applied.

Table 3-1: List of images used in scoring study.

Volunteers were recruited internally within the Churchill Hospital, Oxford, and throughout the UK and USA via the *Medical Physics and Engineering Newsgroup*. Participants were invited to download a ZIP file containing the three images in DICOM format (as well as an additional five images used for a separate study which is not reported here). The ZIP file also included instructions for scoring, and a sheet for recording results. A total of sixteen returns were collected in person and by email between 18th August and 31st October 2011.

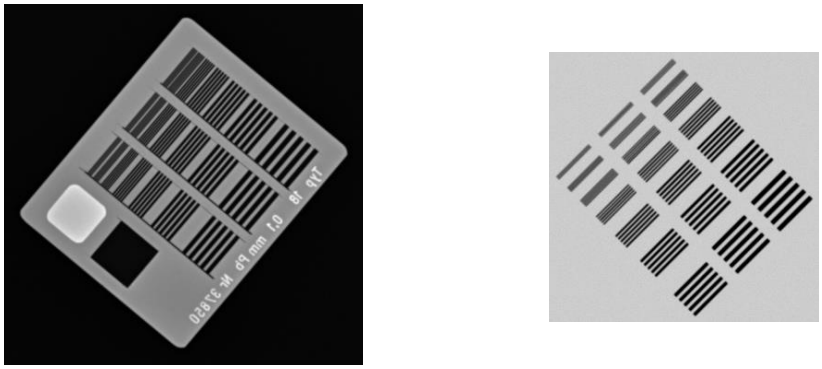

(a) *(b)*

Figure 3-2: Example radiographs showing (a) real Huttner test object and (b) simulated Huttner test object used in scoring studies.

3.3.2 Additional Scoring Study

A smaller scale scoring study was conducted as part of the verification of theoretical derivations discussed in Section 6.4. An image of a simulated Huttner test object (Figure 3-2(b)) was created as described in Section 3.1. Five images were then created by convolving the Huttner phantom with Gaussian PSFs with radii of 0.1, 0.2, 0.3, 0.4 and 0.6 mm, and sampling with a pixel size of 0.2 mm. Poisson noise was added to give the same contrast to noise ratio as Image 1 from the main scoring study (Section 3.3.1). Four volunteers at the Churchill Hospital were asked to score each image using the same protocol as for the main scoring study.

3.4 Quantitative Measurements

Quantitative measurements of the modulation transfer function (MTF) were made using protocols provided by IPEM (IPEM 2010). In order to ensure that the calculation methods were compatible with those which are widely used, the open source package IQWorks was used. This software has been developed by UK hospital physicists and, providing the correct options are selected, implements IPEM recommendations. As the source code is freely available, the algorithms used to calculate MTF can be inspected and, if desired, reproduced in other software.

Measurements of MTF were made using the beam quality defined by IEEE RQA Spectra No.5. This was achieved by adding 21 mm of aluminium filtration to the x-ray

tube, and setting the tube voltage to 92 kV. Following IPEM recommendations (IPEM 2010), the output was set as 1.7 mAs so as to achieve a detector air kerma 3.2 times that which would occur if the automatic exposure controls were used.

A tungsten square with machined edges, shown in Figure 3-3, was used to generate edge response functions. A copper plate without a machine edge was also used for some measurements to provide a comparison. The squares were placed flat on the detector, at angles of approximately 1, 5 and 10 degrees to the pixel matrix, and in various positions. The IQWorks software determined the position of the edge using a Sobel filter and fitted a line function of the form $y = mx + c$. Each pixel value within a 40 x 40 cm region of interest around the edge was then assigned a position on the edge response function by measuring its distance from the line.

The line spread function (LSF) was obtained by differentiating the edge response function numerically. Cubic spline interpolation was then used to up-sample the LSF to 512 points. At this point there was an option to apply a number of windowing functions to minimise aperture effects. The Fast Fourier Transform algorithm was then used to compute the modulation transfer function.

Figure 3-3: Tungsten square used for MTF measurements.

4 Results of Quantitative and Psychophysical Measurements

The resolution of the GE Definium 8000 detector was measured using manual scoring of the Huttner test object and by measuring the MTF directly. The results of these measurements, and the resulting assessment of reproducibility, are presented below.

4.1 Psychophysical Scoring Study

The mean and standard deviations of the returned scores for the three Huttner images are given in Table 4-1. Despite a considerable range in scoring experience and types of monitor used between participants, reasonable agreement was found between the majority of the returns: the mean standard deviation across the three images was approximately 1 line pair group. The IPEM recommended tolerance of 2 line pair groups is therefore approximately equal to two standard deviations of typical inter-scorer reproducibility.

Image Number	Mean (line pair groups)	Standard Deviation (line pair groups)	Two Standard Deviations (line pair groups)	Interpolated Limiting Spatial Resolution (lp/mm)
1	16.6	1.0	2.1	3.0
2	16.1	1.1	2.2	2.8
3	12.1	0.5	1.0	1.8
	Mean	**0.9**	**1.8**	

Table 4-1: Summary of results of scoring study, showing mean and standard deviation of scores for each images, together with the associated LSR.

The most blurred image, image 3, produced scores with a standard deviation approximately half of that of the other two. Given the small dataset it is not possible to confidently ascribe any particular significance to this result. However, it is interesting to note that, for this image, the effect of pixel size, and hence of aliasing, was negligible compared with the pre-sampling resolution. Since the effects of aliasing are often difficult to interpret visually, this suggests that cases where the pre-sampling LSR approaches the Nyquist frequency will tend to result in more uncertainty in scoring.

When only those returns which were scored using calibrated, reporting-quality workstations were considered (a total of 8), the mean scores for the three images decreased to 16.0, 15.5 and 12.0. There is a statistically significant difference (Student t test, $p < 0.05$) between scores obtained on calibrated and uncalibrated monitors. Providing the same type of monitor is always used, systematic difference of this kind are not of particular concern. However, standard deviations for the three images (1, 2 & 3) dropped to 0.8, 0.5 and 0.0 when only calibrated monitors were considered. This indicates that there is some improvement in reproducibility when using calibrated monitors, although greater control for other variables would be required in order to confirm this.

4.2 Quantitative Measurements

The measured edge response function, line spread function and pre-sampling modulation transfer function for the Definium 8000 detector are shown in Figure 4-1. This data was collected using the tungsten square edge placed in the centre of the field. The MTF shown is an average of three MTFs calculated for three radiographs (each acquired with the same exposure factors and without moving the edge).

4.2.1 Repeatability

Repeatability was tested by acquiring three images in succession and processing each separately. The three resulting MTFs are shown on the same graph in Figure 4-2. The difference between the curves is barely perceptible below a spatial frequency of 4 cycles/mm, above which all three profiles become noisy. A quantitative analysis of the variation was performed by measuring the spatial frequencies corresponding to the MTF50 and MTF10 points on each curve. The standard deviations of the frequencies calculated at these points were 0.02 and 0.01 cycles/mm respectively (approximately 0.2% and 0.4%). This suggests that, under standard exposure conditions, the effect of noise fluctuations is small.

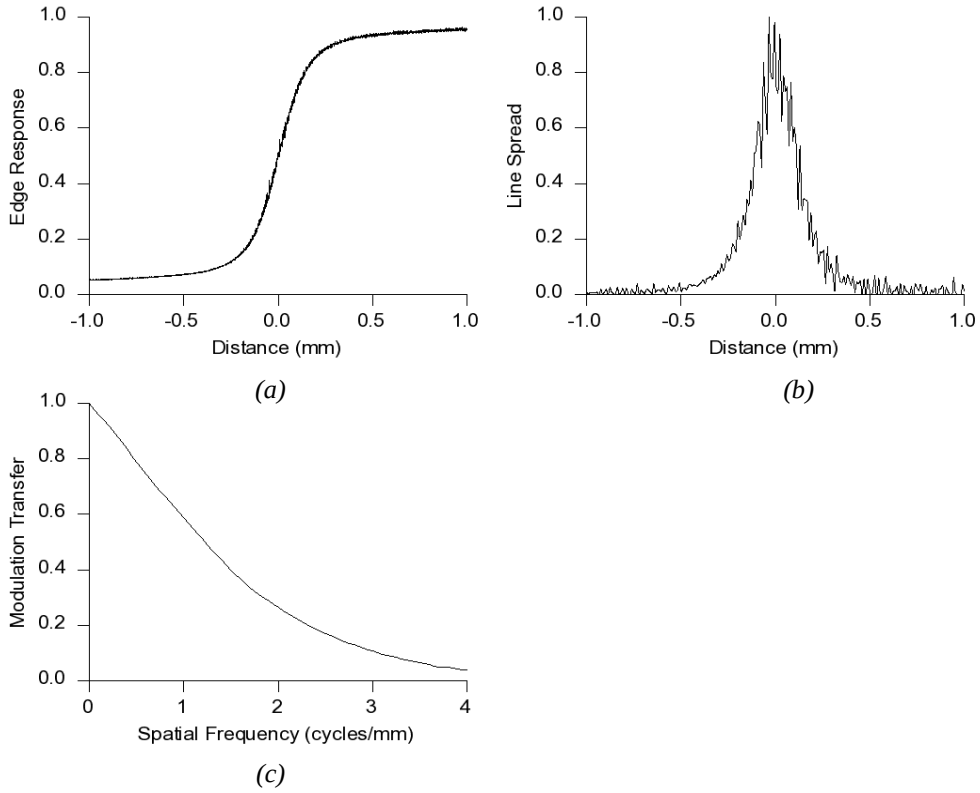

Figure 4-1: Stages of modulation transfer function (MTF) calculation for GE Definium 8000 detector, showing (a) edge response function, (b) line spread function, and (c) MTF. The MTF was averaged over three images.

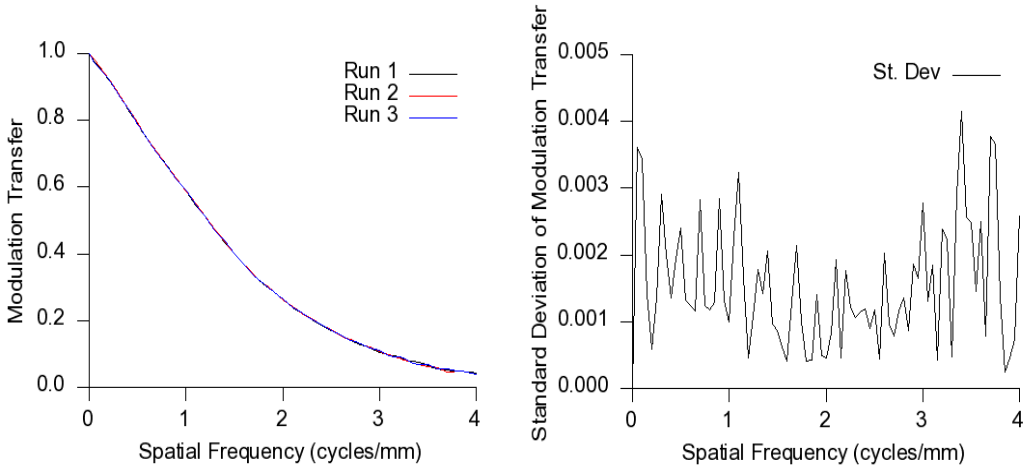

Figure 4-2: Repeatability of MTF measurement where measurement conditions are kept identical. The only contributor to variations is random noise in the radiographs or changes in the output of the x-ray tube between exposures.

4.2.2 Effect of Experimental Set-up

MTFs were calculated with the tungsten edge placed in the four corners of the detector and are compared with the MTF from a centrally placed edge in Figure 4-3(a). Again, it can be seen that there is little difference between the plots, suggesting that for a relatively thin edge material slight changes in the beam angle or heel effect are not particularly significant. The largest changes in MTF50 and MTF10 of 3% occurred for the image taken with the edge in the top left square.

Figure 4-3(b) shows MTFs generated with the tungsten edge placed at angles of approximately 1, 5 and 10 degrees. Visual inspection suggests good agreement up to approximately 4 cycles/mm, beyond which all three profiles become dominated by noise. The range in measured MTF50 and MTF10 spatial frequencies from the three curves is 0.02 cycles/mm. This gives a maximum error of less than 0.5% which is comparable to the base repeatability reported above. It would therefore appear that the method is particularly insensitive to small changes in the angle at which the edge is placed with respect to the pixel matrix.

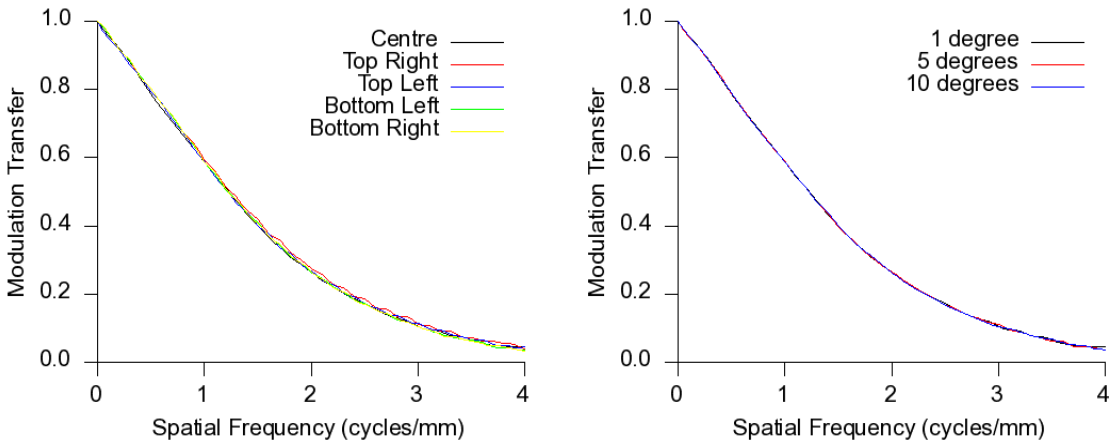

Figure 4-3: Effect of (a) edge position and (b) edge angle on calculated MTF.

An MTF was measured using a square of 1 mm thick copper instead of tungsten. This copper square did not have machined edges, and was slightly deformed following several years of use in quality assurance measurements. Results in Figure 4-4(a) show that the MTF obtained from the copper plate is noisier than that from the tungsten square. This was to be expected, as the contrast of the copper plate was lower than that for the tungsten.

Increasing the size of the region of interest (ROI) reduced the noise to a level comparable with the tungsten, as shown in Figure 4-4(b).

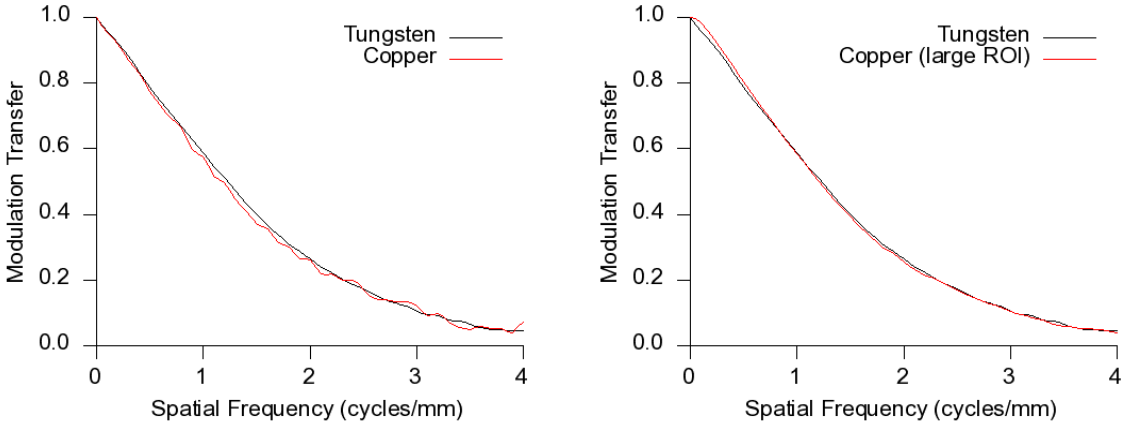

Figure 4-4: (a) Differences between MTF calculated using Tunsten and copper edges. The lower contrast of the copper plate leads to a noisier profile, but this can be countered by increasing the size of the ROI (b).

4.2.3 Effect of Processing

The application of de-noising filters prior to calculating the MTF will clearly have a significant impact if the filter degrades the image resolution. However, given the low nose conditions under which MTF measurements are made, it is unlikely than any such filtering would be required.

A more common processing step is the application of a windowing function on the LSF prior to the Fourier transform. In principle one would like to sample the LSF along an infinitely long profile, but in practice this is limited to the size of the ROI. There is therefore, by default, a rectangular window applied. Since the Fourier transform of a rectangular function is a sinc, this can cause secondary leakage peaks in the MTF (Gibbs ringing). One option to reduce this is to multiply the LSF by one of a number of different windowing functions, and bring the LSF more smoothly towards zero at the edges of the ROI. Examples of such windowing functions include a Gaussian (σ = 0.5), sinc and Hamming; these can be seen in Figure 4-5(a).

Figure 4-5(b) shows the resulting MTF when each of three windows are applied compared with a rectangular window. It can be seen that using a 40 mm long ROI means

that there is no observable benefit to applying a non-rectangular windowing function. This is because the LSF has already dropped below the noise floor by the edge of the ROI. Applying the windowing functions tends to reduce values of the MTF at very low frequencies, as the windows act as a weak high pass filter. The Gaussian window caused the greatest changes in MTF50 and MTF10 of 3% and 2% respectively. This would appear to be relatively large compared with changes due to set up errors and hence there is a need standardise which windowing function, if any, is used.

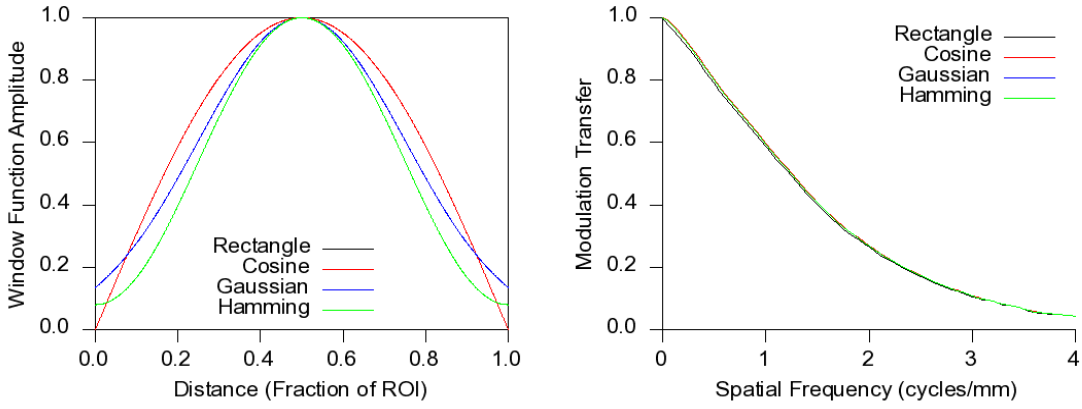

(a) *(b)*

Figure 4-5: (a) Four windowing functions which can be used to minimise ringing artefacts in MTF, and, (b) MTF after windowing functions applied. In this case there is little benefit to applying the windowing functions.

5 Derivation of Relationship Between Tolerances

The purpose of this work was to derive and validate a relationship between Huttner and MTF tolerances. Let us define the spatial frequency $\upsilon_{\lim}$ as the limiting spatial frequency as assessed by an observer scoring the Huttner object. For a given set of noise and observing conditions (which we shall assume to be constant), $\upsilon_{\lim}$ is the value of υ for which $MTF(\upsilon)$ drops below some threshold. We will label this threshold $MTF_{\lim}$, so that $MTF(\upsilon_{\lim}) = MTF_{\lim}$.

Consider first an MTF which is Gaussian. All Gaussian functions can be expressed in the form:

$$MTF(\upsilon) = A\exp\left\{b(\upsilon - c)^2\right\}, \qquad 5\text{-}1$$

where υ is spatial frequency and A, b and c are constants. By definition, $MTF(0) = 1$, and hence $A = 1$. Assuming the MTF is symmetrical about $\upsilon = 0$ requires us to also set $c = 0$, leaving $MTF(\upsilon) = \exp\left\{b\upsilon^2\right\}$.Our definition of $MTF(\upsilon_{\lim}) = MTF_{\lim}$ above is sufficient to determine the constant b in terms of $MTF_{\lim}$ and $\upsilon_{\lim}$:

$$b = \frac{\ln\left[MTF_{\lim}\right]}{\upsilon_{\lim}^{\,2}}, \qquad 5\text{-}2$$

and hence to uniquely define $MTF(\upsilon)$ at all points.

Now consider that the resolution of the system degrades to another Gaussian, $MTF'(\upsilon)$, such that the new limiting resolution (as measured using a Huttner object) is $\upsilon'_{\lim}$. We now have:

$$MTF'(\upsilon'_{\lim}) = MTF_{\lim}. \qquad 5\text{-}3$$

We can obtain an expression for the new value of the MTF at the original $\upsilon_{\lim}$:

$$MTF'(\upsilon_{\lim}) = \exp\left[\frac{\ln(MTF_{\lim})}{\upsilon'^{\,2}_{\lim}} \cdot \upsilon_{\lim}^{\,2}\right], \qquad 5\text{-}4$$

or, as a fractional change from $MTF(\upsilon_{\lim})$:

$$\frac{\Delta MTF(\upsilon'_{\lim},\upsilon_{\lim})}{MTF(\upsilon_{\lim})} = 1 - \frac{\exp\left[\frac{\ln(MTF_{\lim})}{\upsilon'^{2}_{\lim}} \cdot \upsilon^{2}_{\lim}\right]}{MTF_{\lim}}. \qquad 5\text{-}5$$

In general, quality assurance tests do not involve measuring the change in MTF for some value of υ, but rather the change in the value of υ for which $MTF(\upsilon)$ is equal to some constant, k. Typical values for k are 0.5 (50%) and 0.1 (10%), with these points being known as the full-width half maximum, FWHM, and the tenth-width half maximum, TWHM, respectively. We can label the respective values of υ as υ_{50} and υ_{10}, or in general, υ_k.These metrics are also sometimes labelled MTF50 and MTF10.

Before the change in resolution:

$$k = \exp\left[\frac{\ln(MTF_{\lim})\,\upsilon^{2}_{k}}{\upsilon^{2}_{\lim}}\right], \qquad 5\text{-}6$$

and hence:

$$\upsilon_k = \sqrt{\frac{\upsilon^{2}_{\lim}\ln(k)}{\ln(MTF_{\lim})}}, \qquad 5\text{-}7$$

and similarly, after the change in resolution:

$$\upsilon'_k = \sqrt{\frac{\upsilon'^{2}_{\lim}\ln(k)}{\ln(MTF_{\lim})}}. \qquad 5\text{-}8$$

The relative change in υ_k can therefore be expressed as:

$$\frac{\upsilon'_k}{\upsilon_k} = \frac{\sqrt{\frac{\upsilon'^{2}_{\lim}\ln(k)}{\ln(MTF_{\lim})}}}{\sqrt{\frac{\upsilon^{2}_{\lim}\ln(k)}{\ln(MTF_{\lim})}}}, \qquad 5\text{-}9$$

which reduces to:

$$\frac{\upsilon'_k}{\upsilon_k} = \frac{\upsilon'_{\lim}}{\upsilon_{\lim}}. \qquad 5\text{-}10$$

This result means that the fractional change in υ_k with a change in limiting spatial resolution (LSR) is independent of both k and $MTF_{\lim}$. This expression therefore facilitates a trivial conversion between changes in LSR, as measured using a Huttner object, and changes in the reported MTF parameters for the case of Gaussian MTFs.

An important qualification of Equation 5-10 is that it is only useful where the pre-sampling MTF dominates over the effects of pixilation. Where the pixel size dominates (i.e. when the limiting spatial resolution is of the order of the pixel pitch) Equation 5-10 is clearly invalid since the pre-sampling MTF is no longer a suitable predictor of the score which will be assigned to the phantom.

The Huttner-21 object is designed so that the ratio of pitches of adjacent line pair groups is approximate 0.89. This is particularly convenient in the light of Equation 5-10 since it is possible to define a tolerance relationship which is valid for all line pair groups. For a change in resolution of ΔN line pair groups:

$$\frac{\upsilon'_{\lim}}{\upsilon_{\lim}} = (0.89)^{-\Delta N}, \qquad 5\text{-}11$$

and hence:

$$\frac{\upsilon'_k}{\upsilon_k} = (0.89)^{-\Delta N}. \qquad 5\text{-}12$$

5.1 Non-Gaussian MTFs

The above derivation is valid only for a Gaussian MTF, whereas, in general, the MTF may deviate significantly from this form. Equation 5-10 therefore becomes an approximation, the validity of which depends on the local gradient of the MTF relative to the gradient of the Gaussian function at the same point. There is no general form of Equation 5-10 which would hold for all possible MTFs. Equation 5-10 can therefore not be used to relate the LSR and MTF of *any single detector*.

Consider the extreme case example shown in Figure 5-1, where the MTF is essentially flat over the spatial frequencies corresponding to line pair groups 12, 13 and 14. If the last visible group is measured by one observer to be the 14th Group, one would not be surprised to find that a subsequent observer records the last visible group to be 12th Group, since the difference in the CNR (and hence the visibility) of these two groups will be minimal. In this case, applying the IPEM tolerance (two line pair groups) may lead to the erroneous conclusion that a significant change in resolution has occurred. Measurements of the MTF will indicate no change in resolution and hence there is no sensible to way to define an equivalent change in MTF.

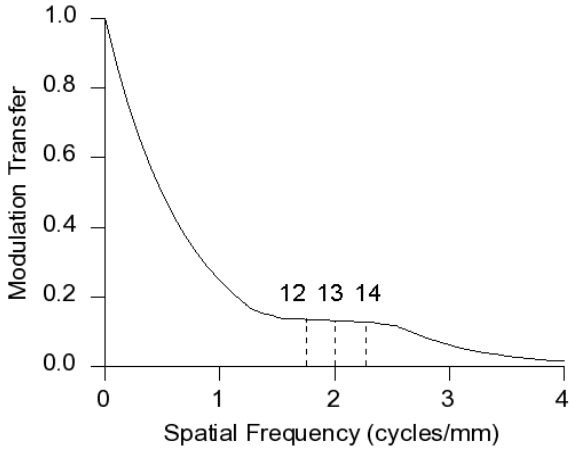

Figure 5-1: Example MTF showing a flat region around 2 cycles/mm. The three Huttner line pair groups with spatial frequencies in this region (no. 12, 13 and 14) are indicated by the dotted lines.

6 Validation of Relationship Between Tolerances

The relationship derived in Section 5 was validated in several ways. Firstly, the assumption that the MTF can be calculated from the SWCF function was verified through computer simulation (Section 6.1). The MTF of the GE Definium 8000 detector was then predicted by analysing Huttner images (Sections 6.4 and 6.2). Finally, the results of the small scoring study (described in Section 3.3.2) were used to check that the change in LSR (as detected by scoring Huttner phantoms) corresponded to the change in MTF indicated by Equation 5-10 (Section 6.3).

6.1 SWCF to MTF Conversion

The theory introduced in Section 2.1.3 suggests that there is a simple, approximate relationship between the square wave contrast function (SWCF) and the MTF at spatial frequencies of the order of the Nyquist limit. This was verified using a computer simulation of an imaging system with properties similar to the GE Definium detector described in Section 3. It was assumed to have a Gaussian pre-sampling PSF with a standard deviation of 0.1 mm (equivalent to a FWHM of 0.24 mm). Since the effects of noise were not modelled in this simulation, other system properties were not relevant.

One dimensional profiles were generated of a square wave function and a sine function, with spatial frequencies ranging from 0.5 to 5 line pairs/mm (equivalent to the Huttner test object), and amplitudes of 1. The effect of the PSF was modelled by convolution with a Gaussian function with standard deviation of 0.1 mm. Initially, a very high sampling rate of 1000 px mm^{-1} was used.

The modulation transfer for each profile was calculated from the range of pixel values between the peaks and troughs of the central four lines, giving the sine wave contrast function and the square wave contrast function (SWCF). The SWCF was then multiplied by the factor of $4\pi/3$ from Equation 2-6 to obtain the Scaled SWCF.

The two resulting modulation transfer functions are plotted in Figure 6-1(a), together with the theoretical MTF obtained from the analytical Fourier transform of a Gaussian function:

$$\Im\left\{\exp\left(\frac{-x^2}{2\sigma^2}\right)\right\} = \exp\left(-2\pi^2 f^2 \sigma^2\right) \qquad 6\text{-}1$$

where x is the spatial co-ordinate, f is the spatial frequency co-ordinate and σ is the standard deviation of the Gaussian (0.1 mm in this case). The plot shows very good agreement between the theoretical MTF and the sine wave contrast function (green line). The scaled SWCF (red line) shows good agreement with the true MTF for higher spatial frequencies, but begins to deviate from it below 1.5 cycles mm^{-1}, as expected.

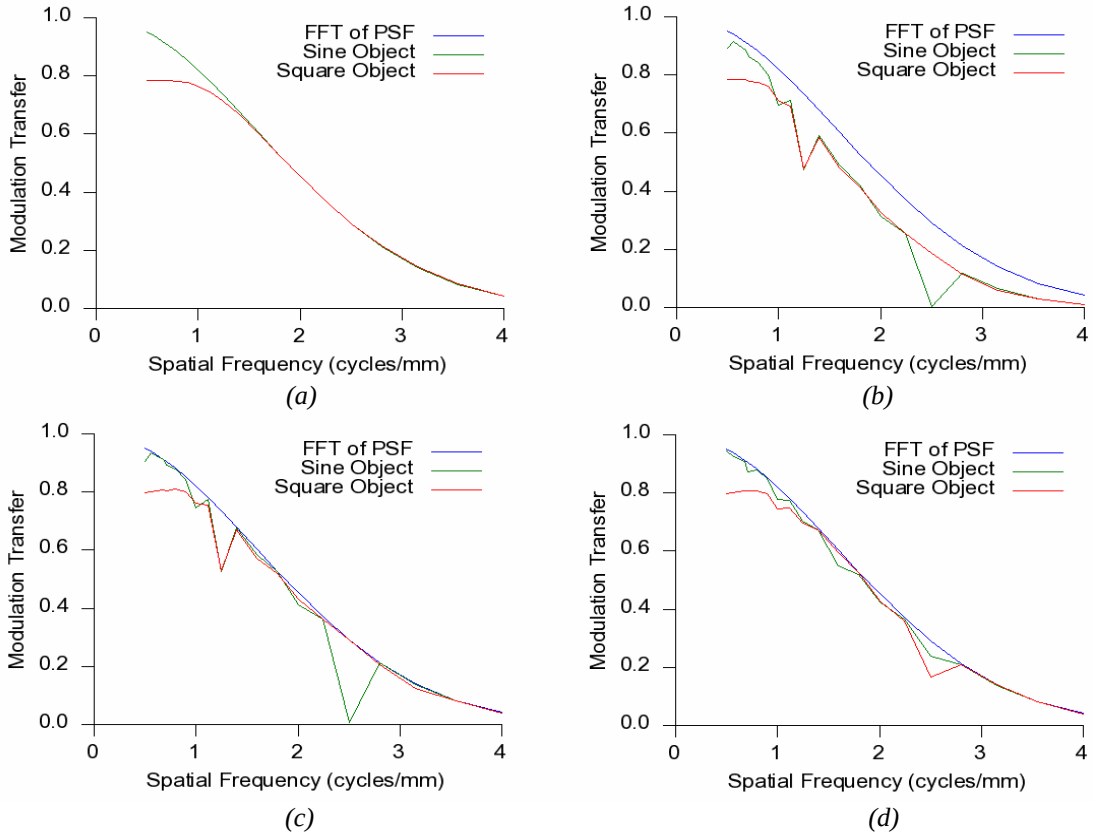

Figure 6-1: MTFs obtained from contrast transfer of sine and square waves and from Fourier transform of the PSF. (a) Sampling rate of 1000 pixels /mm; (b) sampling rate of 5 px/mm, no sinc correction; (c) sampling rate of 5 px/mm, sinc correction; (d) sampling rate of 5 px/mm, sinc correction, 7/10th pixel offset.

The simulation was then repeated with a more realistic pixel size of 5 px mm^{-1}. This was achieved by integrating sections of the profile over lengths of 0.2 mm following convolution with the Gaussian PSF. The resulting profiles are shown in Figure 6-1(b). Since there is now a degradation of resolution due to pixel sampling, the resulting contrast

transfer profiles were multiplied by a factor of $\mathrm{sinc}(\pi f w)$ (where w is the pixel size = 0.2 mm) in order to obtain equivalents to the pre-sampling functions. As can be seen in Figure 6-1(c), this correction achieves a generally good agreement, although deviations can be seen at some spatial frequencies. These are particularly significant at spatial frequencies which are an integer fraction (1/2, 1/4 etc.) of the sampling rate of 5 px mm^{-1}. The variations are also dependent on the offset of the pixel matrix with respect to the image, as demonstrated by Figure 6-1(d) which was produced by shifting the pixel matrix 7/10ths of a pixel with respect to that for Figure 6-1(c).

6.2 Estimation of the MTF of Real Detector using Measured SWCF

Given that the MTF can be obtained from the SWCF for a useful range of spatial frequencies, it should be possible to approximate the pre-sampling MTF of a real detector from the image of a Huttner test object. This was performed for the set of three Huttner images collected for use in the scoring study, as described in Section 3.3. Using ImageJ (an open source image analysis package), a profile was drawn across each of the line pair groups and the maximum and minimum pixel values within (approximately) the four central lines pairs were recorded, giving the contrast for each line pair group. The true contrast (in the absence of any blurring) was taken to be the difference in pixel values between the black background and the white rectangle which can be seen in Figure 3-2. The square wave contrast function (SWCF) for each line pair group was then calculated by dividing the measured contrast by this true contrast.

The SWCF was converted to post-sampling MTF by multiplying by the factor $\pi / 4$ (see Section 2.1.3). An approximation of the pre-sampling MTF was obtained by dividing by the Fourier transform of the pixel function (which was assumed to be a rect), giving the sinc function:

$$\Im\left\{rect\left(\frac{x}{w}\right)\right\} = \mathrm{sinc}\{\pi f w\} \qquad 6\text{-}2$$

where w the pixel width, 0.2 mm. The resulting estimated MTFs from Images 1 and 2 are plotted in Figure 6-2 together with the true pre-sampling MTFs measured using the edge technique described in Section 2.1.5. An order-of magnitude agreement is obtained across a good range of spatial frequencies, demonstrating that the principle of determining the MTF from the Huttner object is sound.

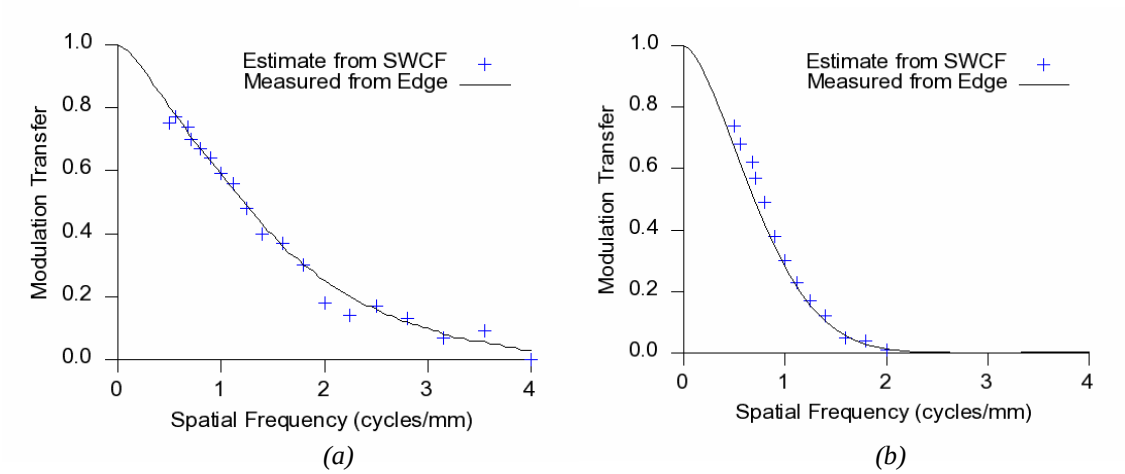

Figure 6-2: MTFs obtained by measured SWCF of Images 1 and 2 from scoring study, compared with MTF obtained using edge method.

An alternative way of measuring the SWCF is to consider the standard deviation of pixel values within each line pair group (IPEM 2010). In principle, this should be less sensitive to noise than the minimum/maximum approach described above. The standard deviations are converted to SWCF by dividing by the mean of the mean pixel values for continuous regions of the two materials making up the line pairs. Conversion to MTF then proceeds as before. The MTF estimated in this way for Image 1 is shown in Figure 6-3; again there is good agreement with the measured MTF. There is a slight systematic over-estimate of the MTF for high spatial frequencies. This may be because stochastic contributions to the standard deviation, which arise due to noise in the image and were not corrected for, become more significant as the modulation transfer becomes small.

It is interesting to note that, despite the detector being slightly under-sampled (the MTF has a value of approximately 0.2 at the Nyquist frequency), there are no apparent affects of aliasing in the SWCF estimate of MTF. This is easily explained by the fact that, within each line pair group, there is likely to be little or no modulation at higher frequencies which can be aliased back. Attempting to apply any sort of correction based on the Expectation MTF (Section 2.1.4) would therefore generate erroneous results.

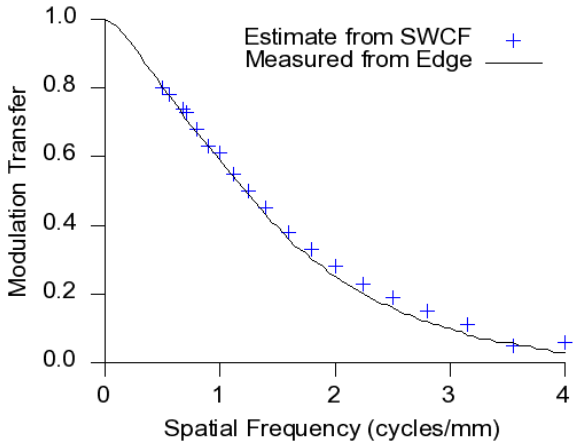

Figure 6-3: MTFs obtained by measuring SWCF (using standard deviations) of Images 1 and 2 from scoring study, compared with MTF obtained using edge method.

6.3 Measurement of Critical CNR for Huttner Test Object

Evaluation of the contrast transfer function as performed above would be an unusual method of scoring images of the Huttner test object. As discussed in Section 2.1.2, when assessing limiting resolution, the observer selects the line pair group with the smallest pitch for which the individual lines can be resolved without aliasing. While such decision making processes are complex, they can be approximated by relatively simple models. For the case of the Huttner scoring problem, the simplest model is to assume that a line pair group is visible by 50% of scorers if the contrast between the lines and the background is greater than some multiple of the image noise.

This is a similar concept to the Rose criterion (Rose 1948) which describes the visibility of discs. However, there are several important differences. The Rose criterion refers to the CNR for the whole object, taking into account its size. In this case, only the pixel CNR is considered. Therefore, the value calculated may be specific to a particular size or arrangement of test patterns. The importance of calculating the critical CNR therefore lies not in being able to define an absolute value, but in checking for consistency between different MTFs when the same object is imaged.

Using this model, the scoring process can be characterised by determining some critical value of CNR for which the observer will conclude that the lines are discernible. An estimate of this critical CNR was made using returns from the scoring study discussed in Section 3.3.1. The calculated CNRs of the last visible group for each of three images are given in Table 6-1. The mean CNR of the last visible group was approximately 12. For

Image No. 1, which had noise properties closest to those expected for the IPEM recommended exposure parameters, the limiting spatial resolution is equivalent to the point at which the MTF has dropped to 10%. This suggests that measuring the MTF at tenth-maximum is likely to give results which are most closely related to limiting spatial resolution.

Image No.	Average Score	Spatial Frequency of Scored Group (lp/mm)	MTF at Spatial Frequency of Scored Group	Noise	Contrast to Noise Ratio of Scored Group
1	16.6	3.01	0.09	16.4	14.4
2	16.1	2.835	0.06	11.3	11.0
3	12.1	1.82	0.03	6.4	9.6

Table 6-1: Contrast to Noise Ratios (CNRs) of line pair groups which correspond to the average Huttner score for three Huttner Images. Each image had different resolution and noise properties due to the application of Gaussian filters: σ = 0.1 mm pixel for Image 2, and σ = 0.2 mm for image 3.

6.4 Verification using Simulated Huttner Images

A simple verification of Equation 5-10 was performed by asking volunteers to score a set of six simulated Huttner images with varying MTF. The pre-sampling MTF for each image was generated analytically and the full width tenth maximum (FWTM) spatial frequency was calculated. This allowed the fractional change in spatial frequency, $\Delta\upsilon_{10}/\upsilon_{10}$, to be calculated between each image and the next. Equation 5-12 was then used to calculate the expected change in the FWTM spatial frequency from the observer scoring of the Huttner object. It can be seen from Table 6-2 that there is a reasonably good agreement for the cases where the pre-sampling resolution is poor and hence where it dominates over the pixel size (given that the main scoring study suggests an uncertainty of 1 line pair group on observer scoring). For the cases with better pre-sampling resolution, it is the pixel size which determines the limiting spatial resolution and hence Equation 5-10 has poor predictive power. In these cases, the MTF will predict a larger change in visible group than is actually observed.

Image No.	Gaussian SD (mm)	Mean Score	Change in TWHM (mm^{-1})		Change in Last Visible Group Number	
			Measured from MTF	Predicted from Score	Predicted from MTF	Measured from Score
1	0.10	16.0				
2	0.15	14.3	0.33	0.18	3.5	1.7
3	0.20	13.0	0.25	0.14	2.5	1.3
4	0.25	11.7	0.20	0.14	2.0	1.3
5	0.30	10.0	0.17	0.18	1.5	1.7
6	0.35	9.0	0.17	0.18	1.3	1.0

Table 6-2: Results of testing tolerance conversion using small scoring study. The change in MTF tenth width half maximum (TWHM) is predicted from the change in observer score of the Huttner object, and the change in observer score is predicted from the change in TWHM. SD = standard deviation.

7 Conclusions

It has been demonstrated that there is an approximate physical equivalence between pre-sampling MTF and Huttner line pair group visibility when effects due to finite pixel size do not dominate. In the case of constant noise, the LSR can be predicted from the MTF. It is therefore feasible to convert existing LSR tolerances to MTF tolerances for the purposes of maintaining consistency between the two tests. The relationship between these two tolerances is given by:

$$\frac{\upsilon'_k}{\upsilon_k} = \frac{\upsilon'_{\lim}}{\upsilon_{\lim}}, \qquad 7\text{-}1$$

where $\upsilon_{\lim}$ and $\upsilon'_{\lim}$ are the old and new (Huttner measured) limiting spatial resolutions respectively, and $\frac{\Delta\upsilon_k}{\upsilon_k}$ is the fractional change in the spatial frequency for a given amplitude on the MTF curve (for example the tenth-maximum).

For the Huttner-21 test object used in this study, this can be simplified to:

$$\frac{\Delta\upsilon_k}{\upsilon_k} = (0.89)^{-\Delta N}, \qquad 7\text{-}2$$

where ΔN is the change in the number of the last resolvable line-pair group. For any non-Gaussian MTF, this relation will not be exact, and hence it would be inappropriate to use it to compare LSR and MTF for any single detector.

IPEM currently (IPEM 2006) recommends a remedial tolerance of two line pair groups for Huttner measurements for fluoroscopic and computed radiography detectors, and a tolerance of 25% in limiting spatial resolution for direct digital detectors. Analysis of the data in Table 2-1 shows that, on average, a change in visibility of two line pair groups is equivalent to a change in limiting spatial resolution of 26%. Hence these two tolerances can be considered to be broadly equivalent.

Data collected from the scoring study (Section 4.1) suggests that a standard deviation of one line pair group can be expected when different observers score the same image. It would not be possible to reduce the tolerance from two to one line pair groups without experiencing a number of spurious failures. The tolerance on the Huttner method is

therefore limited by uncertainties in observer scoring rather than any fundamental properties of the detector.

Using Equation 5-12, the Huttner tolerance of 2 line pair groups can be shown to be equivalent to a tolerance of approximately 20% for MTF values such as MTF50 and MTF10. The results of Section 3.4 suggest that this level of MTF tolerance would be very unlikely to be breached providing that reasonable care is taken to ensure that measurements and processing is consistent between tests. Results of the scoring study suggest an uncertainty of approximately 1 line pair group when scoring the Huttner object. If this can be considered to represent the limit of human perceptibility of changes in resolution, then there is an argument for using the equivalent MTF tolerance of approximately 11%.

For MTF measurements, IPEM Report 32 (IPEM 2010) suggests using remedial and suspension level MTF50 tolerances of 0.2 mm^{-1} and 0.4 mm^{-1} respectively. Since these tolerances are expressed as absolute rather than as fractional changes, they cannot be directly converted to a change in line pair groups using Equation 5-12. However, if the example of the Definium 8000 detector is taken, for which the MTF50 spatial frequency is 1.23 mm^{-1}, then the percentage tolerances become 16% and 32%. The remedial tolerance suggested by IPEM would therefore appear to be slightly tighter than the Huttner remedial tolerances for this detector.

There is no suggestion that any of the equivalent tolerances derived here are necessarily the most appropriate for use with an MTF based test. LSR tolerances are based on the experimental uncertainty inherent in psychophysical measurements, uncertainties which are significantly reduced when quantitative metrics are used. The results reported in Section 4.2 indicate that the MTF tolerance could be set significantly tighter without significant risk of spurious failures, providing that reasonable care is taken to ensure reproducibility of measurement conditions.

Decisions on tolerances must be taken at local level, and no definitive external guidance can be provided. However, the work presented here should be of some assistance to medical physics departments as they select and justify their choice of tolerances. A better understanding of the relationship between psychophysical and quantitative metrics for detector resolution can only encourage greater adoption of the MTF into routine quality assurance programmes.

References

Beutal J 2000 Handbook of medical imaging: Physics and psychophysics, Volume 1 *SPIE Press* p548

Burgess AE 1999 The Rose model, revisited *J. Opt. Soc. Am. A* **16** 633-646

Campbell F W and Robson J G 1968 Application of Fourier analysis to the visibility of gratings *J. Physiol.* **197** 551-566

Chesters M S and Hay G A 1983 Quantitative relation between detectability and noise power *Phys. Med. Biol.* **28** 1113-1125

Cohen G, McDaniel D L and Wagner L K 1984 Analysis of variations in contrast-detail experiments *Med. Phys*. **11** 469-473

Coltman J W 1954 The specification of imaging properties by response to a sine wave input *J Opt. Soc. Am.* **44** 468

Cunningham I A 2008, Use of the detective quantum efficiency in a quality assurance program *Proc SPIE* **6913** 691331

Cunningham I A 1991 Signal and noise in modulation transfer function determinations using the slit, wire, and edge techniques, *Med. Phys*. **19** 1037

Dobbins J T III, Samei E 2006 Intercomparison of methods for image quality characterization. II. Noise power spectrum *Med. Phys*. **33** 1466-1475

Dobbins JT III 1995 Effects of undersampling on the proper interpretation of modulation transfer function, noise power spectrum, and noise equivalent quanta of digital imaging systems *Med. Phys.* **22** 171

Doyle P 2009 Assessment and optimisation of digital radiography systems for clinical use *PhD Thesis*, University of Glasgow

Good W F, Gur D, Feist J H, Thaete F L, Fuhrman C R, Britton C A and Slasky B S 1994 Subjective and objective assessment of image quality – a comparison Journal of *Digital Imaging* **7** 77

Goodman J W 2005 Introduction to Fourier Optics *Roberts and Company Publishers* p22-25

Fujita H Tsai D Y Itoh T Doi K Morishita J Ueda K Ohtsuka A 2002 A Simple method for determining the modulation transfer function in digital radiography *IEEE Transactions on Medical Imaging* **11** 34-39

IPEM 2005 Report 91: Recommended standards for the routine performance testing of diagnostic x-ray imaging systems *IPEM, York*

IPEM 2010 Report 32 Part VII: Measure of the performance characteristics of diagnostic x-ray systems: digital imaging systems *IPEM, York*

Kotre C J 1998 Effect of background structure on detection of low contrast objects in mammography *Br. J. Rad*. **71** 1162

Launders J H, Kengyelics S M and Cowen A R 1998 A comprehensive physical image quality evaluation of a selenium based digital x-ray imaging system for thorax radiography *Med. Phys* **25** 986

Lawinski C, Mackenzie A, Cole H, Blake P and Honey I 2005 Report 05078: Digital Detectors for General Radiography. A comparative technical report. *NHS Purchasing Supply Agency, Centre for Evidence Based Purchasing*

Loo L N D, Doi K, Metc CE 1984 A comparison of physical image quality indices and observer performance in the radiographic detection of nylon beads *Phys. Med. Biol.* **29** 837-856

Marshall N W 2006 A comparison between objective and subjective image quality measurements for a full field digital mammography system *Phys. Med. Biol*. **51** 2441-2463

Marshall N W 2007 Early experience in the use of quantitative image quality measurements for the quality assurance of full field digital mammography x-ray systems *Phys. Med. Biol*. **52** 5545-5568

Marshall N W 2009 Detective quantum efficiency measured as a function of energy for two full-field digital mammography systems *Phys. Med. Biol*. **54** 2845-2861

Marshall N W Mackenzie A and Honey I D 2011 Quality control measurements for digital x-ray detectors *Phys. Med. Biol.* **56** 979

Metz C E, Wagner R F, Doi K, Brown D G, Nishikawa R M and Myers K J 1994 Toward consensus on quantitative assessment of medical imaging systems *Med. Phys*. **22** 1057-1061

Metz C E, Doi K 1979 Transfer function analysis of radiographic imaging *systems Phys. Med. Biol.* **24** 1079-1106

Myers K J, Barrett H H, Borgstrom M C, Patton D D and Seeley G W 1985 Effect of noise correlation on detectability of disk signals in medical imaging *J. Opt. Soc. Am. A* **2** 1752-1759

NHS 2007 Cost effectiveness of direct digital radiography versus computed radiography

for chest examinations *Purchasing and Supply Agency, Centre for Evidence Based Purchasing*

Nill N B 2001 Conversion between sine wave and square wave spatial frequency response of an imaging system *Mitre Technical Report* MTR 01B0000021

Reilly A J 2010 A uniform framework for the objective assessment and optimisation of radiotherapy image quality *PhD Thesis* University of Edinburgh

Rong X J, Shaw C C, Liu X, Lemacks M R, Thompson S K 2011 Comparison of an amorphous silicon/cesium iodide flat-panel digital chest radiography system with screen/film and computed radiography systems - A contrast-detail phantom study *Med. Phys.* **28** 2328

Rose A 1948 The sensitivity performance of the human eye on an absolute scale *J. Opt. Soc. Am* **38** 196-208

Samei E, Ranger N T, Dobbins J T and Chen Y 2006 Intercomparison of methods for image quality characterization. I. Modulation transfer function *Med. Phys.* **33** 1454

Samei E and Flynn M J 2003 An experimental comparison of detector performance for direct and indirect digital radiography systems *Med. Phys.* **30** 607

Schober H A W and Hilz R 1965 Contrast sensitivity of the human eye for square wave gratings *J. Opt. Soc. Am.* **55** 1086-1090

Siewerdsen J H, Antonuk L E, El-Mohri Y, Yorkston J, Huang W and Cunningham I A 1998 Signal, noise power spectrum, and detective quantum efficiency of indirect-detection flat-panel imagers for diagnostic radiology *Med. Phys*. **25** 614-628

Shannon C E 1949 Communication in the presence of noise *Proc. Inst. Rad. Eng.* **37** 10-21

Suetans P 2002 Fundamentals of medical imaging *Cambridge University Press* p5